

Influence of pump bandwidth on the efficiency of side-pumped, double-beam mode-controlled lasers: establishing a new record for Nd:YLiF₄ lasers using VBG

Niklaus U. Wetter^{1,*} and Alessandro M. Deana²

¹Center for Lasers and Applications, Instituto de Pesquisas Energeticas e Nucleares - IPEN, 2242 Av. Prof. Lineu Prestes, São Paulo, Brazil

²Department of Biophotonics Applied to Health Sciences, Universidade Nove de Julho - UNINOVE, 235 Vergueiro St, São Paulo, Brazil
nuwetter@ipen.br

Abstract: We analyze the performance of a VBG equipped diode of narrow linewidth in a side-pumped double-beam, mode-controlled resonator and demonstrate power scaling without loss of beam quality by a factor of three, when compared to previous results. 69 W of diffraction-limited laser output power at 1053 nm in a Nd:YLF lasers are demonstrated with slope efficiency of 65% and record optical-to-optical efficiency of 60%.

©2015 Optical Society of America

OCIS codes: (140.3410) Laser resonators; (140.3530) Lasers, neodymium; (140.3580) Lasers, solid-state.

References and links

1. E. H. Bernhardt, A. Forbes, C. Bollig, and M. J. D. Esser, "Estimation of thermal fracture limits in quasi-continuous-wave end-pumped lasers through a time-dependent analytical model," *Opt. Express* **16**(15), 11115–11123 (2008).
2. Y. Hirano, T. Yanagisawa, S. Ueno, T. Tajime, O. Uchino, T. Nagai, and C. Nagasawa, "All-solid-state high-power conduction-cooled Nd:YLF rod laser," *Opt. Lett.* **25**(16), 1168–1170 (2000).
3. G. Aka, L. Zheng, A. Ikesue, Y. Aung, and P. Loiseau, "CW intracavity frequency doubled Nd:YAG core ceramics composite at 473 nm," in Proceedings of Conference on Advanced Solid State Lasers, OSA Technical Digest (Optical Society of America, 2014), paper AM4A.3.
4. R. S. Pinto and N. U. Wetter, "Highly efficient, dynamically stable Nd:YAG single-rod resonators with 60% TEM₀₀ extraction efficiency and high misalignment stability," *Laser Phys.* **24**(8), 085801 (2014).
5. A. Minassian, B. Thompson, and M. J. Damzen, "Ultrahigh-efficiency TEM₀₀ diode-side-pumped Nd:YVO₄ laser," *Appl. Phys. B* **76**(4), 341–343 (2003).
6. N. U. Wetter, E. C. Sousa, F. A. Camargo, I. M. Ranieri, and S. L. Baldochi, "Efficient and compact diode-side-pumped Nd:YLF laser operating at 1053 nm with high beam quality," *J. Opt. A, Pure Appl. Opt.* **10**(10), 104013 (2008).
7. N. U. Wetter and A. M. Deana, "Diode-side-pumped Nd:YLiF₄ laser emitting at 1053 nm with 53.6% optical efficiency and diffraction-limited beam quality," *Laser Phys. Lett.* **10**(3), 035807 (2013).
8. N. U. Wetter and A. M. Deana, "Power scaling of a side-pumped Nd:YLF laser based on DBMC technology," *Appl. Phys. B* **117**(3), 855–860 (2014).
9. A. M. Deana, I. M. Ranieri, S. L. Baldochi, and N. U. Wetter, "Compact, diode-side-pumped and Q-switched Nd:YLiF₄ laser cavity operating at 1053 nm with diffraction limited beam quality," *Appl. Phys. B* **106**(4), 877–880 (2012).
10. M. Deana and N. U. Wetter, "High-efficiency, Q-switched and diffraction-limited Nd:YLF side-pumped laser," *Proc. SPIE* **8433**, 84330B (2012).
11. A. M. Deana, E. C. Sousa, I. M. Ranieri, S. L. Baldochi, and N. U. Wetter, "1kHz repetition rate, mode-controlled, passively Q-switched Nd:YLF laser operating at 1053 nm," *Proc. SPIE* **8235**, 82350G (2012).
12. A. M. Deana, M. A. P. A. Lopez, and N. U. Wetter, "Diode-side-pumped Nd:YLF laser emitting at 1313 nm based on DBMC technology," *Opt. Lett.* **38**(20), 4088–4091 (2013).
13. N. U. Wetter, E. C. Sousa, I. M. Ranieri, and S. L. Baldochi, "Compact, diode-side-pumped Nd³⁺:YLiF₄ laser at 1053 nm with 45% efficiency and diffraction-limited quality by mode controlling," *Opt. Lett.* **34**(3), 292–294 (2009).

14. B. L. Volodin, S. V. Dolgy, E. D. Melnik, E. Downs, J. Shaw, and V. S. Ban, "Wavelength stabilization and spectrum narrowing of high-power multimode laser diodes and arrays by use of volume Bragg gratings," *Opt. Lett.* **29**(16), 1891–1893 (2004).
15. Y. Wang, T. Kasamatsu, Y. Zheng, H. Miyajima, H. Fukuoka, S. Matsuoka, M. Niigaki, H. Kubomura, T. Hiruma, and H. Kan, "Cesium vapor laser pumped by a volume-Bragg-grating coupled quasi-continuous-wave laser-diode array," *Appl. Phys. Lett.* **88**(14), 141112 (2006).
16. R. H. Page, R. J. Beach, V. K. Kanz, and W. F. Krupke, "Multimode-diode-pumped gas (alkali-vapor) laser," *Opt. Lett.* **31**(3), 353–355 (2006).
17. K. Kubodera and K. Otsuka, "Single-transverse-mode LiNdP₄O₁₂ slab waveguide laser," *J. Appl. Phys.* **50**(2), 653–659 (1979).
18. Y.-F. Lü, X.-H. Zhang, A.-F. Zhang, X.-D. Yin, and J. Xia, "Efficient 1047 nm CW laser emission of Nd:YLF under direct pumping into the emitting level," *Opt. Commun.* **283**(9), 1877–1879 (2010).
19. J. A. Caird, S. A. Payne, P. R. Staber, A. J. Ramponi, L. L. Chase, and W. F. Krupke, "Quantum electronic properties of the Na₃Ga₂Li₃F₁₂:Cr³⁺ laser," *IEEE J. Quantum Electron.* **24**(6), 1077–1099 (1988).

1. Introduction

Pump schemes for diode pumped solid state laser (DPSSLs) are traditionally divided into longitudinal- and side-pumped DPSSLs. In longitudinally pumped designs, the pump is coaxial to the optical axis of the resonator, which produces good overlap between pump and laser beam, favoring efficient extraction of the pump energy with good laser beam quality. Drawbacks of this design, especially for high power applications, are limited power scalability and expensive, fiber-coupled pump diodes [1]. The other approach, diode side-pumping, is very advantageous in terms of power scaling because several diode side-pump modules can be accommodated within the same resonator. Additionally, these diodes can be simple bars or stacked bars and, therefore, high pump powers can be imaged economically into the active volume of the laser rods.

In a side-pumped system, the overlap efficiency between pump and laser beam is lower in comparison to end-pumped schemes because the highest pump inversion generally does not coincide spatially with the highest intensity of the laser mode. For example, in a side-pumped rod configuration, a very high inversion is achieved at the barrel surface, far away from the center of the rod. However, even during multimode operation, no oscillating transversal mode will benefit from the high inversion at this surface due to diffraction losses. Some authors have tried to mitigate this problem by inserting a neodymium doped YLiF₄ (YLF) rod into an MgF₂ prism or by sintering a small Nd:YAG rod into an undoped YAG cylinder [2,3]. Ideally, in the absence of losses at the interface between doped and undoped cross-sections, in such a composite rod the laser mode can be bigger than the doped section of the rod, generating good overlap between pump inversions and transversal oscillating mode. Besides the constructional complexity of a transversally composite rod, there still remains the problem that the doped cross-section should be ideally close to one millimeter in diameter if the desired transversal mode is to be of high quality (TEM₀₀ mode or fundamental transversal mode operation). The reason is that larger doping sections will require larger fundamental modes, which in turn decrease the overlap of the tangential and radial stability zones of the resonator that are caused by the thermal lensing inside the Nd:YAG rod [4]. As a consequence of the small diameter of the doped section, absorption will be incomplete, decreasing efficiency for fundamental mode operation. The transversally composite rod design probably will become equally efficient as the techniques described further below once ceramic sintering techniques become available for materials of very high absorption cross-section such as neodymium doped vanadate.

For materials with high absorption coefficient, such as Nd:YVO₄ or Nd:GdVO₄ when pumped at the peaks of the 800 nm absorption band, the pump beam is fully absorbed within a short depth. Thus a single grazing incidence of the laser beam at the pump face may efficiently screen the pump inversion, leading to the highest efficiencies so far reported for operation at room temperature [5]. This so-called "bounce resonator" employs two cylindrical intracavity lenses which increase the aspect ratio of the fundamental transversal mode along the pump direction for good overlap. Materials with lower absorption coefficient, such as

Nd:YLF crystals, will operate inefficiently and in multi-mode within a bounce resonator and, therefore require a new approach in order to obtain high efficiency [6].

The double-beam-mode-controlling (DBMC) technique has solved the efficiency problem for lesser absorbing crystals by letting the laser beam undergo a total internal reflection (TIR) at the pump surface with a smaller incidence angle, travelling therefore deeper inside the crystal where there is still population inversion [7]. Moreover, the technique also introduces a folding mirror that creates a second TIR for the laser beam, displaced from the position of the first TIR by a certain distance, in order to efficiently screen the inversions at the pump facet. The controlled gain competition between the two near-parallel beams inside the slab guarantees stable TEM₀₀ mode operation even at high diode pump powers above 100 Watt, without inserting additional losses [8].

In addition, this approach requires no cylindrical intracavity optics to create highly elliptical beams which are necessary with other techniques [5]. A Nd:YLF based on the DBMC design resulted in 53.6% optical-to-optical efficiency (63.5% slope efficiency), which is the highest optical efficiency ever reported for a Nd:YLF laser pumped around 800 nm, including multimode operation, operation at the higher gain line (1047 nm) and end-pumped schemes [7]. The design has shown to be power scalable, operable at different laser lines and capable of delivering efficient Q-switched operation at kHz-level repetition rate [8–12].

The side-pumped design requires that the laser beam size is well matched to the absorption coefficient in order to be efficient and of fundamental mode [13]. All off-axis pump inversion must be screened or else higher order transversal modes will start to oscillate. When the pump bandwidth becomes comparable to the width of the absorption peak, the lowly absorbed pump frequencies may travel far off-axis causing multi-mode operation. Regular laser diode arrays show at least 2 - 3 nm spectral bandwidths (FWHM) which is comparable to the absorption peak of Nd:YLF at 797 nm. A diode equipped with volume Bragg grating (VBG), which has a bandwidth of only 0.5 nm, should therefore fare better [14]. VBG equipped diode bars have already been used as pump source for alkali vapor lasers (DPAL) and for direct pumping into the emitting level of neodymium doped vanadates [15, 16].

In this work we demonstrate the operation of a Nd:YLF laser pumped with a regular diode at the 792 nm absorption peak and compare to pumping with a VBG equipped diode at 797 nm. With the narrow bandwidth VBG equipped diode a new efficiency record for diode pumped Nd:YLF lasers is established.

2. Experimental setup

The a-cut Nd:YLF crystal (Crystech, China) has 1 mol% of neodymium doping level and all surfaces were polished and uncoated. Its dimension is 13 mm x 13mm x 3 mm and the c-axis is orientated perpendicular to the large cooling facets [Fig. 1(a)]. The crystal is placed in a copper housing with top and bottom water cooling. The duty cycle was kept at 5% to avoid thermal fracture and the pump pulse duration was 350 μ s. The resonator had two highly reflecting mirrors, one flat (M2) and one curved folding mirror (M3) with 3 m radius of curvature (ROC). The transmission of the flat output coupling mirror (M1) was 20%. The first pump diode (Coherent, USA) had its peak emission at 792 nm when operated at 27° C and required an additional AR-coated half wave plate after the fast axis collimating lens to rotate polarization of the output beam by 90° in order to access the crystal's highly absorbing π -polarization [Fig. 1(a)]. The second diode (Northrop Grumman, USA) had a VBG after the fast axis collimating lens in order to tune the spectral peak to 797.0 nm and narrow the bandwidth to 0.5 nm FWHM, as shown in Fig. 2. In all cases the diode beam was focused into the crystal by a $f = 20$ mm spherical lenses, resulting in spot size of approximately 4 mm width and 0.1 mm height.

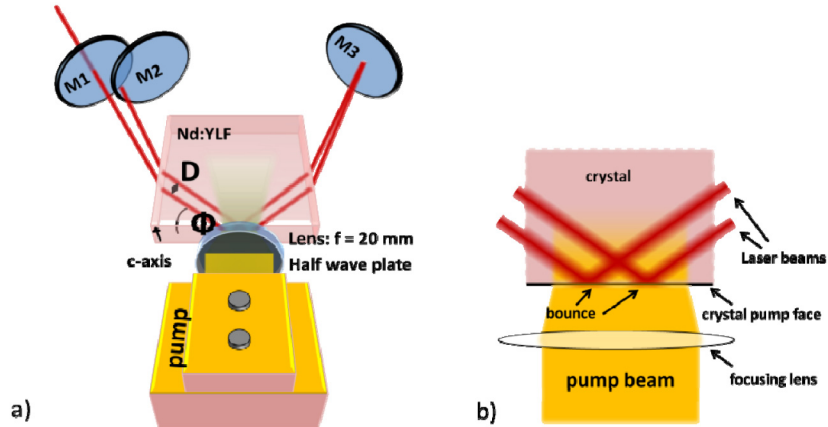


Fig. 1. Schematic diagram of the DBMC laser cavity (a) and detail of the pump region (b). M2 (flat) and the curved folding mirror M3 (3 m ROC) are highly reflecting mirrors. The flat output coupling mirror M1 has 20% transmission.

After the focusing optics and Fresnel reflections at the uncoated pump facets, about 88.5% of the pump power was effectively absorbed by the slab.

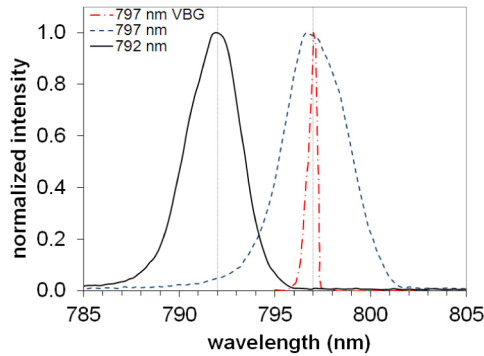


Fig. 2. Emission spectrum of the two pump sources used in this work. To the left the 792 nm diode, to the right the VBG equipped 797 nm diode. For comparison a standard 797 nm diode bar without VBG (dotted line) is also shown.

3. Simulations

When calculating a laser resonator, a constant absorption coefficient is generally assumed. This simplification generally works well for end-pumping schemes because all pump frequencies are absorbed deeper inside the crystal by the same collinear, transversal oscillating mode. However, as pointed out before, this is not the case for side-pumped resonators where population inversion in a deeper region of the active medium may easily cause oscillation of new and higher order modes.

Figure 3(a) shows a simulated diode laser spectrum assuming an ideal pump beam with a Gaussian spectrum and 0.01 nm bandwidth (FWHM) emitting at 792 nm (25°C). The measured (Cary 5000, resolution of 0.2 nm), π -polarized absorption spectrum of our crystal is shown in Fig. 3(b). As can be seen in Fig. 3(b), the 1 mol% Nd:YLF absorption spectrum contains several peaks at 792 nm, 797 nm and 806 nm. The highest peak of 8 cm^{-1} is at 797 nm. This peak is 50% narrower (approx. 2.6 nm FWHM) than the peak at 792 nm (approx. 5.2 nm FWHM), which is composed of two nearby absorption levels $^4F_{5/2} + ^2H_{9/2}$. Both peaks are much wider when compared to the simulated diode emission of 0.01 nm FWHM. Figure 3(c) shows the fraction of absorbed power (isoquant curves) as a function of the distance from

pump facet (y-axis) and the diode temperature (x-axis) for the 0.01 nm FWHM diode. This cross-correlation graph is obtained by taking the normalized diode spectrum recorded at its design temperature (normally 25°C) and at a specific operating current, then translating this spectrum in frequency by the diode's temperature dependent frequency shift (0.22 nm/°C) and calculating the overlap with the crystal spectrum for each operating temperature.

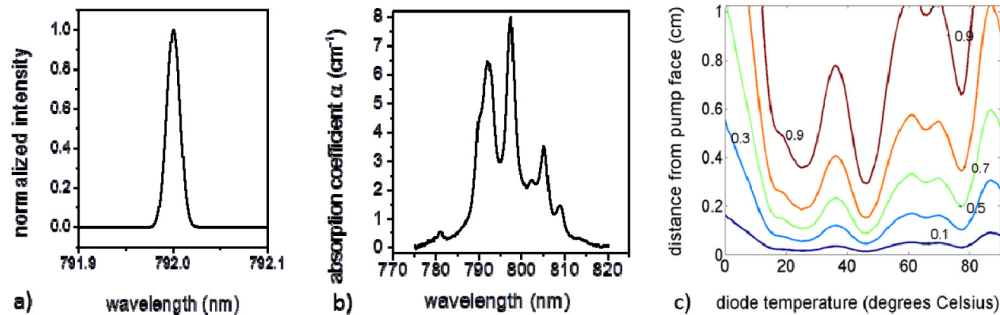


Fig. 3. a) simulated diode emission; b) measured crystal absorption spectrum of a 1mol% Nd:YLF crystal; c) absorption isoquant curves as a function of distance from pump facet (y-axis) and diode temperature (x-axis). Each curve represents a fraction of absorbed pump power indicated by its number.

Figure 3(c) shows the local absorption inside the crystal when the diode is operated at the different absorption peaks of 792 nm and 797 nm, which are emitted at diode temperatures of 25°C and 45°C, respectively. In Fig. 3(c) it can be observed that the isoquant curves follow closely the crystal spectra, showing good absorption at 25°C, corresponding to the 792 nm emission of the diode, higher absorption at 45 °C (797 nm) and another, lower absorption peak at ~75°C, corresponding to the 806 nm absorption peak in Nd:YLF. To absorb 90% of the pump radiation, a crystal length of approximately 4.5 mm would be necessary at 25°C (792 nm) diode temperature whereas only 3 mm are necessary at 45°C (797 nm).

Although the x-axis scale in Fig. 3(c) shows very high temperatures it should be noted that it is not convenient to operate a real diode at temperature below the dew point or above 45°C and that a real diode's spectral features change when operated far off from its design temperature.

Real diode bars have larger bandwidth, generally at least 2 nm to 3 nm. Even if such a diode is temperature tuned to the absorption peak of the crystal, a considerable amount of the diode emission contained in the off-center part of its spectrum does not coincide with the crystal peak absorption, therefore experiences a smaller absorption coefficient. The emission spectrum of the 792 nm diode used in our experiment and the respective cross-correlation graph are shown in Figs. 2 and 4(a), respectively. Comparing Figs. 4(a) and 3(c) shows that, although the 797 nm absorption peak is higher than absorption at 792 nm, the broader bandwidth of the latter peak results in an equally good absorption of real pump diodes, independent on the emission being at either 792 nm (25°C) or 797 nm (45°C), as demonstrated in references [7,12]. Approximately 90% of the pump light of the 792 nm diode is absorbed in 5 mm of crystal length (Fig. 4(a)), which is 2/3 longer than what we would need using the idealized diode of Fig. 3(a) at 797 nm (3mm, Fig. 3(c) at 45°C).

For comparison purposes we also simulated the VBG equipped diode as if its thermal wavelength shift were 0.22 nm/°C. This serves to show if such a diode would work better at 792 nm or at 797 nm. In reality the thermal wavelength shift of VBG equipped diodes is about 0.007 nm/°C and depends on the temperature of the VBG and not on the temperature of the diode. It would therefore not be possible to temperature tune a 797 nm VBG diode to 792 nm. However, using above assumption, the simulation of the VBG equipped diode is shown in Fig. 4(b) and it can be observed that it does fare better in terms of absorption than the 792 nm

diode, almost as good as the idealized diode of Fig. 3(a), furthermore, the absorption is bigger at 797 nm and the crystal absorbs 90% in 3.5 mm length.

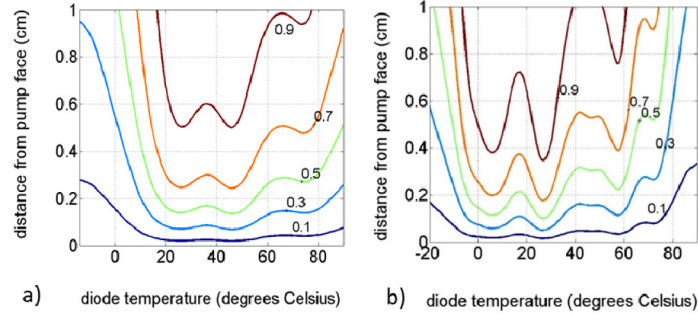


Fig. 4. a) absorption isoquant curves as a function of distance from pump facet (y-axis) and diode temperature (x-axis) for the 792 nm diode (a) and the VBG equipped diode (b).

Because off-center frequencies are less absorbed, they travel further into the crystal until eventually the remaining pump energy only contains lesser absorbed spectral components. In order to illustrate the consequences of this behavior we introduce a local effective absorption coefficient for the pump radiation that is a function of the penetration depth into the crystal. The fraction of absorbed pump power contained within a segment d of the crystal situated at a distance L from the pump face is given by

$$F(T, L) = \int D(\nu, T) \left\{ e^{-C(\nu)L} - e^{-C(\nu)(L+d)} \right\} \delta\nu \quad (1)$$

where $D(\nu, T)$ is the normalized diode spectrum taken at temperature T and $C(\nu)$ is the crystal spectra. The negative logarithm of $F(T)$ divided by L is the effective absorption coefficient:

$$\alpha_{\text{eff}}(T, L) = -\ln F(T, L) / L \quad (2)$$

In Fig. 5 the effective absorption coefficients for all three diodes are plotted as a function of L , the third diode being the assumed ideal pump beam of 0.01 nm FWHM only used for simulations. It is clearly seen that only this ideal, extremely small bandwidth diode has the same absorption coefficient throughout the crystal (and therefore shows single exponential absorption throughout the crystal), whereas all the real diodes decrease in terms of effective absorption with crystal depth. The VBG equipped diode, that presents a bandwidth (of 0.5 nm) does have lower values of α_{eff} and decreases by 15% when L reaches 1 cm. The 792 nm diode with bandwidth of 3 nm shows a 30% smaller initial absorption and also decays faster, showing a more than 25% decrease by the time it reaches 1 cm of crystal depth. The decrease of the effective absorption coefficient with crystal length is due to the fact that only lesser absorbed frequencies penetrate deep into the crystal. In Fig. 5(b) the total absorbed pump power as a function of crystal length is shown. This figure shows that the difference between the 0.01 nm linewidth diode and the 0.5 nm, VBG diode is very small when compared to a standard diode.

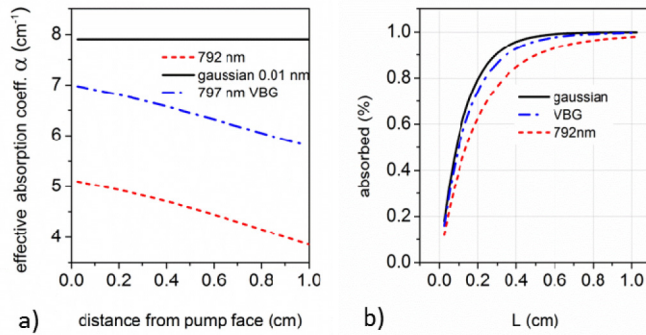


Fig. 5. local effective absorption coefficient for the three simulated diodes (a) and the percentage of absorbed pump power as a function of L (b).

Using a space dependent MATLAB code based on reference [13] that calculates the output power and the threshold of higher order transversal modes as a function of overlap between spatial population inversion and laser mode distribution, we calculated the sloped efficiency and the maximum power at which TEM₀₀ mode is still maintained without co-oscillation of higher order modes [17].

The parameters that most strongly influence the outcome of these simulations are the absorption coefficient [Fig. 3(b)] and the beam waist in the pump direction, which is 550 μm and almost constant throughout the cavity given the long ROC of our folding mirror [12].

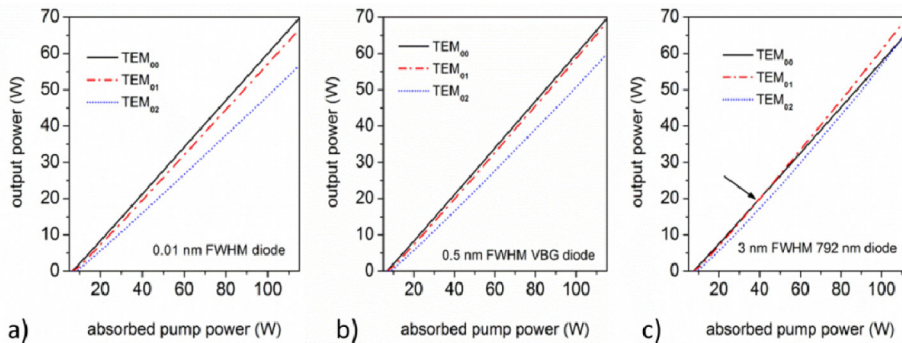


Fig. 6. Simulated input- output power curves for the three diodes, the narrow linewidth (a), the 797 nm VBG (b) and the standard 792 nm (c).

Figure 6 shows the simulated input-output power curves for the three diodes. Graph (a) shows the 0.01 nm linewidth diode (diode 1), graph (b) shows the 797 nm diode with VBG (diode 2) and graph (c) shows the standard 792 nm diode (diode 3). The simulations also show at which pump power the laser becomes multimode and if the next rectangular transverse mode to operate has (TEM₀₂) or does not have (TEM₀₁) a central lobe. As long as the TEM₀₀ mode has the higher output power at a fixed pump power, no multimode oscillation will occur. Once another mode overtakes the TEM₀₀ mode, both modes will oscillate simultaneously.

With all three diodes the laser starts to oscillate in TEM₀₀ mode (black line). However the separation between the TEM₀₀ mode and the TEM₀₁ mode is smaller with diode 2 than with diode 1, which indicates that at higher pump powers (> 115 W) the laser will probably work multimode. Slope efficiency and optical to optical efficiency are the same in both cases and of 65% and 60%, respectively. Diode 3 becomes multimode at approximately 40 W of pump power (optical efficiency of 53%) with two transversal modes operating (TEM₀₀ and TEM₀₁, see downward arrow in Fig. 6(c)) and three transversal modes (TEM₀₀, TEM₀₁ and TEM₀₂,

see upward arrow in Fig. 6(c)) operating at approximately 110 W. This last result is in close agreement with the experimental data from [7].

Figure 6 shows the main results of this simulation and explains why in previous works we were limited to lower pump powers. It becomes clear that in this side-pumped set-up the linewidth of the pump diode is a key issue for achieving very high output powers while maintaining the excellent beam quality.

3. Results and discussions

The laser threshold was 8 W of pump power and the maximum power fluctuation, after a few minutes of warm-up time, was less than 2% over a test period of 4 h [Fig. 7(a)]. Optimum results were obtained by using a 20% transmission output coupler at 1053 nm. At the maximum available absorbed pump power of 115 W, the output power was 69 W, with diffraction limited beam quality [Fig. 7(b)]. In comparison with the previous result ([7], circles in Fig. 7(a)), we obtained an even higher optical-to-optical efficiency of $60 \pm 2\%$, establishing a new record, even in comparison with end-pump schemes [18]. The slope efficiency of the laser was 65% (trend of Fig. 7(a)). In terms of input pump power the efficiency numbers are 4% lower compared to absorbed pump power, given the absence of anti-reflection coating on the crystal pump face. Caird's analysis was carried out and resulted in resonator losses of 1.4% and the photon - to - photon conversion efficiency of 83% [19].

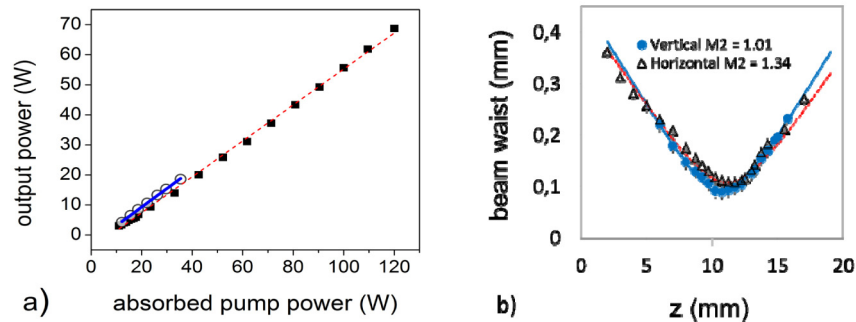


Fig. 7. a) output power in TEM₀₀ mode as a function of absorbed pump power using the VBG-equipped diode (squares) and the 792 nm diode from [7]. The lines represent a linear regression considering all experimental data. b) beam profile and M² measurements of the DBMC laser

Figure 7(b) shows the beam profile along with the M² fit. M² values of 1.01 and 1.34 were obtained in the vertical and horizontal directions, respectively, using the second moment method. The measurement was done at the highest pump power. The excellent beam quality shows that, even at very high intracavity powers, multimode oscillation is avoided by the DBMC technique. This is in part due to the fact that the technique is equivalent to a soft aperture for higher order modes [6]. As already pointed out, the maximum pump power at which this soft aperture can still avoid the oscillation of higher order modes is limited. In previous work on DBMC technology, we were limited to 35 W of pump power before multimode operation as shown in Fig. 7(a) [7]. One possible means to overcome this value is choosing a larger beam waist [8,12]. In [8], Wetter et al, we used a folding mirror of 10 m, which results in a beam waist of approximately 600 μm, with the result that we could pump with more than 100 W maintaining fundamental mode operation and excellent beam quality.

Also seen in Fig. 7(a) is that the experimental slope efficiency of both lasers is practically the same although the effective absorption coefficient due to the 792 nm diode is 30% smaller (Fig. 5(a)). This is also in agreement with the simulations in Figs. 6 (b) and (c) that show the same slope efficiency for both cases (up to 40 W) and also show that the 792 nm pumped resonator becomes multimode close to 40W of pump power.

The reasons why both resonators show the same slope efficiency, although there is a big difference in effective absorption (30%, Fig. 5(a)), has to do with the overlap between inversion volume and the two beams used in the double-beam mode-controlling technique shown in Fig. 1(b). As long as both beams effectively cover the inversion area there is no difference in slope efficiency independent on absorption coefficient. In that case it does not matter if 90% of the pump power is absorbed in 3 mm (idealized 0.01 nm FWHM diode), 3.5 mm (VBG-diode) or 5 mm (standard 792 nm diode) of crystal length [Figs. 3(c), 4(a), 4(b)] as demonstrated by experiment [Fig. 7(a)] and simulations [Figs. 6(b) and (c)].

However, at high pump powers (in excess of 40 W) and low effective absorption coefficients (as with the 792 nm diode), there is enough energy deposited deeper inside the crystal to allow for higher order modes in spite of the soft aperture effect of the DBMC technique. This energy deposit in deeper crystal regions is not only due to the lower initial effective absorption shown in Fig. 5(a) (5 cm^{-1} for the 792 nm diode) but is also further enhanced due to the not single-exponential absorption of Eq. (2) that brings additional energy to this deeper regions by means of off-center frequencies in the diode spectrum. The effect is observed in the simulation of Fig. 6(c) when accompanying the TEM_{00} mode (black line) as a function of pump power: For the lower part of pump powers the slope efficiency is excellent and only TEM_{00} mode oscillation occurs, however, it then starts to roll over at high pump powers and the slope efficiency becomes clearly worse allowing also for multimode oscillation.

The advantage of using a VBG-equipped diode is, therefore, a higher dynamic range of TEM_{00} operation and consequently, higher TEM_{00} output power. In this work, the input power range at which fundamental mode could be maintained without loss of efficiency was increased by a factor of more than three, from 35 W to 115 W of pump power.

4. Conclusions

Side pumped resonators that use TIR at the pump face for the laser beam traditionally rely on large TEM_{00} modes and highly absorptive laser crystals in order to guarantee fundamental transversal mode operation. For a given product of absorption coefficient times beam waist, there exists an upper pump power limit after which the laser becomes multimode. Here we analyze for the first time the performance of a VBG equipped diode of narrow linewidth in such a resonator and demonstrate power scaling without loss of beam quality by a factor of three, when compared to previous results. We demonstrate 69 W of laser output power at 1053 nm with a slope efficiency of 65% and a new record optical-to-optical efficiency of 60% for Nd:YLF lasers. Additionally, the traditional excellent beam quality of Nd:YLF lasers can be maintained during power scaling as shown by the M^2 value of 1.17 average, obtained in this work.

Acknowledgments

We would like to thank the São Paulo Research Foundation FAPESP for Grant No. 2012/11437-8.